Society of Medical Education & Research

2026, Volume 6, Issue 1, Page No: 207-226

ISSN: 3108-4834

Archive of International Journal of Cancer and Allied Science

The Role of Hsa_circ_0136666 in Promoting Gastric Cancer Progression and Tumor Immune Escape through Regulation of the miR-375/PRKDC Axis and PD-L1 Phosphorylation

Erik Van der Meer[1]*, Lieke Jansen[1], Bram de Vries[2], Sophie Claes[3]

[1]Department of Gastric Cancer and Circular RNA Biology, Faculty of Medicine, Wageningen University, Wageningen, Netherlands.

[2]Department of Tumor Immune Escape and PD-L1 Regulation, Faculty of Medicine, University of Groningen, Groningen, Netherlands.

[3]Department of miRNA and PRKDC Axis in Cancer, Faculty of Medicine, University of Amsterdam, Amsterdam, Netherlands.

***E-mail** ✉ e.vandermeer@wur.nl

Abstract

Conventional targeted therapies have shown limited success in extending survival for gastric cancer patients, primarily owing to off-target toxicities and mechanisms of tumor immune evasion. Circular RNAs are abundantly present in tumor tissues, serving as potential biomarkers and promising therapeutic targets. The role of hsa_circ_0136666 in driving gastric cancer cell proliferation was examined using Western blotting, quantitative real-time PCR (qRT-PCR), fluorescence in situ hybridization (FISH), and flow cytometry. Tumor immune evasion processes in tumor-bearing mouse models were assessed using tissue immunofluorescence, enzyme-linked immunosorbent assay (ELISA), and flow cytometry. Differential expression of circRNAs in clinical specimens was evaluated via tissue microarray FISH. The ability of siRNA to enhance the effectiveness of anti-PD-L1 therapy and modulate the immune microenvironment was tested using co-administration. We showed that hsa_circ_0136666 is broadly and strongly expressed in gastric cancer tissues and cell lines. Functionally, it stimulated tumor cell proliferation and shaped the tumor microenvironment, facilitating immune escape in a manner reliant on CD8+ T cells. Mechanistically, hsa_circ_0136666 acted as a sponge for miR-375-3p, thereby elevating PRKDC levels. This led to PD-L1 phosphorylation, which prevented its degradation, promoted PD-L1 clustering, and suppressed immune activity, ultimately weakening anti-tumor immune responses. Therapeutically, LNP-delivered siRNA significantly boosted the efficacy of anti-PD-L1 agents and curtailed immune evasion. These findings highlight the tumor-promoting role of hsa_circ_0136666 in gastric cancer, driving PD-L1 phosphorylation via the miR-375/PRKDC pathway, thereby enabling immune escape. The study identifies a novel pathogenic mechanism in gastric cancer, positions hsa_circ_0136666 as a new immune-related target, and offers a foundation for improving anti-PD-L1 treatment outcomes in this malignancy.

Keywords: Circular RNA, miR-375, PD-L1, Immune escape, Gastric cancer

Introduction

Gastric cancer represents a major global health challenge due to its elevated incidence and mortality rates across numerous regions. It accounts for more than 700,000 deaths each year and ranks as the third most common cause of cancer-related death worldwide [1]. Clinical symptoms typically emerge only in advanced stages, complicating timely diagnosis [2, 3]. Existing treatments are constrained by patient comorbidities, acquired drug resistance, and adverse effects, falling short of clinical needs [4]. Consequently, there is an urgent demand for reliable early diagnostic markers and more effective therapeutic approaches for gastric cancer (GC).

Circular RNAs (circRNAs) constitute a class of abundant, highly stable non-coding RNAs distinguished

Access this article online https://smerpub.com/

Received: 17 March 2026; **Accepted:** 12 June 2026

How to cite this article: Van der Meer E, Jansen L, de Vries B, Claes S. The Role of Hsa_circ_0136666 in Promoting Gastric Cancer Progression and Tumor Immune Escape through Regulation of the miR-375/PRKDC Axis and PD-L1 Phosphorylation. Arch Int J Cancer Allied Sci. 2026;6(1):207-26. https://doi.org/10.51847/G0UL8urREG

by their covalently closed circular structures [5, 6]. They exert key regulatory effects by sponging miRNAs, modulating transcription, interacting with RNA-binding proteins, influencing protein activity, or even producing small peptides [7]. Growing evidence links circRNAs to various conditions, including diabetes, neurological disorders, cardiovascular diseases, and malignancies [8, 9]. In particular, circRNAs have been implicated in the molecular processes underlying gastric carcinogenesis [10, 11]. A primary mechanism involves their interaction with microRNAs (miRNAs), allowing them to competitively bind miRNA response elements and thereby derepress miRNA target genes [12].

MicroRNAs (miRNAs), like circRNAs, are prevalent non-coding RNAs that post-transcriptionally repress gene expression by binding to target mRNAs [13]. Prior work from our group demonstrated that miR-375 is downregulated in gastric cancer and functions as a tumor suppressor [14, 15].

The rationale for this investigation centered on circPRKDC. PRKDC encodes the catalytic subunit of DNA-dependent protein kinase (DNA-PK), which is essential for repairing DNA double-strand breaks and facilitating recombination [16]. Beyond its role in DNA repair, PRKDC acts as a versatile protein kinase that phosphorylates diverse substrates to regulate their functions [17]. Immune checkpoint proteins, such as PD-L1, undergo multiple post-translational modifications—including phosphorylation, palmitoylation, and ubiquitination—that influence their stability and activity [18-20] and contribute to tumor progression [21, 22].

In this research, we identified hsa_circ_0136666 as highly upregulated in gastric cancer, where it sponges miR-375. Through this axis, hsa_circ_0136666 upregulates PRKDC expression, leading to PD-L1 phosphorylation and stabilization. This cascade promotes the progression of gastric cancer and facilitates immune evasion.

Materials and Methods

Human tissue specimens

The study included 21 cases of gastric cancer with recurrence and metastasis (7 cases with primary tumor/adjacent normal tissue/metastasis, 5 cases with primary tumor/adjacent normal tissue, 5 cases with primary tumor/metastasis, and 4 cases with metastasis only) along with 5 cases of normal human gastric mucosa, for a total of 50 clinicopathological specimens. The Ethics Committees of Shandong University, Taizhou Hospital, and Shanghai Outdo Biotech Company approved the research protocol.

Cell culture and transfection

GES-1, MKN-45, and MFC cells were cultured in RPMI-1640 medium, while HEK-293T cells were maintained in Dulbecco's Modified Eagle Medium (DMEM; KeyGEN, China). All cell lines were obtained from the Cell Bank of the Chinese Academy of Sciences and cultured in medium supplemented with 10% fetal bovine serum (FBS; LONSERA, Shanghai, China) at 37 °C in a 5% CO_2 incubator. AGS cells were purchased from the same source and cultured in AGS-specific medium (Procell, CM-0022). Cells used in the experiments were in the logarithmic growth phase and had undergone no more than 20 passages. Transfections of siRNAs, miRNA mimics, and plasmids were performed using jetPRIME® reagent (Polyplus-transfection, New York, USA).

Actinomycin D assay

Cells were treated with DMSO (vehicle) or 2 μg/mL Actinomycin D (APExBIO, USA) to inhibit transcription for 2, 4, 8, or 12 hours. QRT-PCR was then used to quantify expression levels of hsa_circ_0136666 and its linear counterpart PRKDC mRNA.

Ribonuclease R (RNase R) digestion

One microgram of total RNA was incubated at 37 °C for 10 minutes with or without 1 U/μg RNase R (Geneseed, Guangzhou, China) following the manufacturer's protocol. Samples were subsequently reverse-transcribed into cDNA, and qRT-PCR was used to measure expression of hsa_circ_0136666 and PRKDC mRNA.

RNA Fluorescence in Situ Hybridization (FISH)

Cy3-labeled probes for miR-375 and FITC-labeled probes for hsa_circ_0136666 and PRKDC mRNA were used for RNA FISH. Probes for miR-375 and PRKDC mRNA were designed and synthesized by GenePharma (Shanghai, China), while the hsa_circ_0136666 probe was obtained from Geneseed (Guangzhou, China). Hybridization was performed in MKN-45 cells for hsa_circ_0136666 & miR-375 and miR-375 & PRKDC mRNA pairs. Cell slides fixed with 4% paraformaldehyde were processed according to the RNA-FISH Kit (GenePharma) protocol. After denaturation at 73 °C for 5 minutes, the probe mixture was hybridized overnight at 37 °C in the dark. Images were acquired

using a laser confocal microscope and viewed/exported with CaseViewer software.

RNA isolation and quantitative reverse transcription-PCR (qRT-PCR)

Total RNA from cells and tissues was extracted using TRIzol reagent (TransGen Biotech, Beijing, China). For mRNA and circRNA quantification, RNA was reverse-transcribed using HiScript III RT SuperMix (R323-01, Vazyme). qPCR was performed with ChamQ Universal SYBR qPCR Master Mix (Q711-02, Vazyme). miRNA reverse transcription was carried out using M-MLV (H-) Reverse Transcriptase (R021-01, Vazyme). Expression levels were normalized to GAPDH (for circRNA/mRNA) or U6 snRNA (for miRNA) using the 2^−ΔΔCt method. All experiments were performed in at least three independent replicates.

CD8+ T cell co-culture assay

CD8+ T cells were isolated from mouse spleens using the MojoSort™ Mouse CD8+ T Cell Isolation Kit (catalog 480007, BioLegend). Isolated cells were activated with Ultra-LEAF™ Purified anti-mouse CD3ε/CD28 antibodies (catalog 100339/102115, BioLegend) for 3 days per the manufacturer's instructions. Co-culture experiments were conducted in RPMI-1640 medium supplemented with IL-2 (10 ng/mL). Lentivirus-transfected cancer cells were seeded and allowed to adhere overnight before incubation with activated CD8+ T cells for 48 hours. The effector-to-target ratio ranged from 1:1 to 1:20. After incubation, T cells and debris were removed by PBS washes, and viable cancer cells were quantified by crystal violet staining and absorbance at 595 nm.

Luciferase reporter assay

HEK-293T cells were co-transfected with hsa_circ_0136666 or mutant hsa_circ_0136666, miR-375 mimics or miR-NC, PRKDC 3'UTR or mutant PRKDC 3'UTR, along with pMIR-Report vector. After 48 hours, luciferase activity was measured using the Duo-Lite Luciferase Assay System (Vazyme, China) according to the manufacturer's protocol. Firefly luciferase (560 nm) and Renilla luciferase (480 nm) signals were detected with a multifunctional microplate reader (i3x).

RNA-binding protein immunoprecipitation (RIP)

RIP assays were performed using Protein A/G Agarose Resin (Bimake, USA) following the manufacturer's instructions. MKN-45 cells were co-transfected with relevant constructs (hsa_circ_0136666 or mutant, miR-375 mimics or miR-NC, PRKDC 3'UTR or mutant). Forty-eight hours post-transfection, cells were lysed in NP-40 buffer (Beyotime, China). After centrifugation, supernatants were incubated with anti-AGO2 antibody. Protein-A/G beads were added for 3 hours to capture the complexes. Immunoprecipitated RNA was extracted and analyzed by qRT-PCR.

Cell viability assay (Cell counting kit-8)

Cell proliferation was evaluated using the CCK-8 assay (Target Mol, USA). MKN-45 and AGS cells were transfected with the hsa_circ_0136666 plasmid or siRNA using jetPRIME. Cells were seeded at 2,000 cells per well in 100 µL medium in 96-well plates and incubated at 37°C with 5% CO_2 for 24 hours. Then, 10 µL of CCK-8 solution was added to each well and incubated for 1 hour. Absorbance was measured at 450 nm using a microplate reader.

Western blotting and co-immunoprecipitation

Total protein was extracted with RIPA buffer (EpiZyme, Shanghai, China) and quantified using the BCA Protein Assay Kit (YEASEN, China). SDS-PAGE gels were prepared with the PAGE Gel Fast Preparation Kit (EpiZyme). Membranes were incubated with primary antibodies overnight at 4 °C.

Enzyme-linked immunosorbent assay (ELISA)

Tumor tissues were weighed and homogenized in saline at a 1:9 (weight: volume) ratio under ice-water bath conditions. Levels of IL-6, TGF-β1, and IFN-γ were measured according to the instructions of the corresponding mouse ELISA kits (Multiscience). Standard curves were generated using linear fitting.

Use of siRNA and preparation of LNP

siRNA (Biomics) was encapsulated into lipid nanoparticles (LNP) using lipid components dissolved in ethanol at molar ratios of 50:10:38.5:1.5 (ionizable lipid: DSPC: cholesterol: PEG-lipid). The lipid mixture was combined with 10 mM citrate buffer (pH 4.0) containing siRNA at a 1:3 volume ratio (lipids: siRNA) via a NanoAssembler system (Suzhou Wenhao Microfluidic Technology Co., Ltd., China). Formulations were concentrated using Amicon Ultra-15 ultrafiltration units.

Control siNC and target siRNAs/shRNAs were synthesized by Biomics Biotech.

Animal model construction and treatment protocol

In general, C57BL/6 or BALB/c nude mice were subcutaneously injected with tumor cells. Once tumors reached approximately 100 mm^3 in volume, tumor dimensions were measured regularly, and treatment was initiated. An anti-mouse PD-L1 monoclonal antibody was administered by intraperitoneal injection at 2 mg/kg every 3 days. LNP-siRNA was delivered by direct intratumoral injection at a dose of 40 μg siRNA (or siNC control) per mouse in a volume not exceeding 100 μL. Injections were performed every three days, with timing staggered relative to anti-PD-L1 administration. The cell line-derived xenograft (CDX) model followed standard subcutaneous tumor implantation procedures.

Flow cytometric analysis of mouse tumors

Mice were euthanized by cervical dislocation. Tumors were carefully excised using surgical instruments sterilized with 75% ethanol. Excised tumors were minced into small fragments with sterile ophthalmic scissors and digested with 0.25% trypsin for 10–20 minutes. Single-cell suspensions were obtained by passing the digested material through a 300-mesh nylon filter two to three times. Cell concentration was adjusted to approximately 5×10^5 cells/mL. The resulting suspensions were stained with appropriate antibodies for at least 20 minutes, according to established protocols. Stained cells were analyzed on a BD FACS Celesta flow cytometer (BD Biosciences). Data analysis was performed using FlowJo software.

Statistical analysis

All experiments were independently repeated at least three times unless otherwise specified. Quantitative results are expressed as mean ± standard deviation (SD). Statistical comparisons between groups were conducted using unpaired Student's t-test with SigmaPlot software (version 12.0). Significance levels were denoted as follows: *P ≤ 0.05, **P ≤ 0.01, ***P ≤ 0.001, ****P ≤ 0.0001. Graphs were prepared using GraphPad Prism (version 8.3.0) or FlowJo (version 10).

Results and Discussion

Hsa_circ_0136666 interacts with miR-375 and correlates positively with gastric cancer progression

Previous investigations revealed that miR-375 suppresses gastric cancer development. We observed that forced expression of miR-375 induced significant alterations in various long non-coding RNAs, including circRNAs. This suggested that upstream regulators might control endogenous miR-375 activity. To pinpoint potential miR-375-sponging circRNAs, we analyzed differentially expressed circRNAs from the Gene Expression Omnibus (GEO) dataset GSE147698. This analysis identified 1,466 circular RNAs that were significantly altered ($P < 0.05$, fold change > 1.2), of which 1,262 were upregulated **(Figure 1a)**. Among these upregulated candidates, we further screened for those containing miR-375 binding sites using the ENCORI database (rnasysu.com/encori/index.php). Both circPRKDC and its linear counterpart PRKDC were found to harbor miR-375 binding sites. Notably, hsa_circ_0136666 emerged as the primary circPRKDC isoform capable of binding miR-375. This circRNA, spanning chr8:48,715,866–48,730,122 in the human genome, arises from back-splicing of exons 68-70 of the PRKDC gene, resulting in a 477-nucleotide circular transcript **(Figure 1b)**. Divergent primers were used to amplify the back-splice junction. Sanger sequencing of the PCR products verified the presence of hsa_circ_0136666 in gastric cancer cells **(Figure 1c)**.

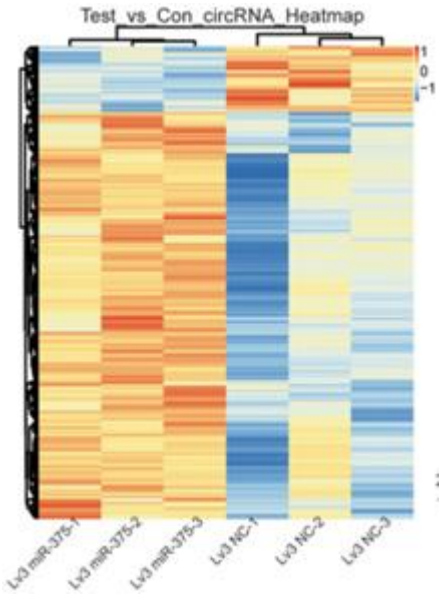

a)

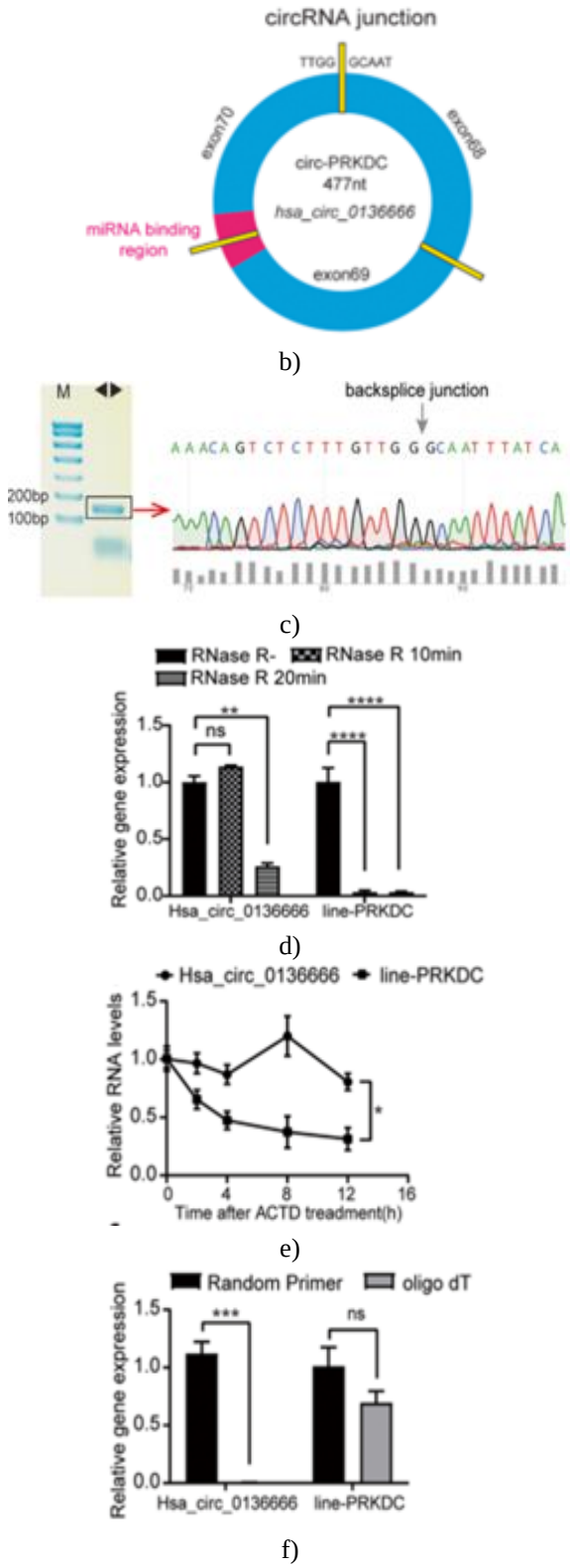

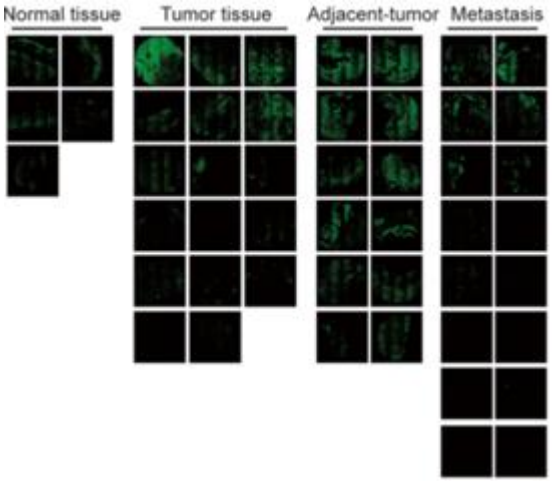

Figure 1. Hsa_circ_0136666 interacts with miR-375 and shows positive association with gastric cancer progression

(a) hsa_circ_0136666 is prominently represented among the differentially expressed transcripts identified in the gene chip analysis; (b) Schematic representation illustrating the biogenesis of hsa_circ_0136666; (c) Divergent primers were employed for amplification, followed by Sanger sequencing of the resulting PCR products; (d) Expression levels of hsa_circ_0136666 and its linear PRKDC counterpart were compared following RNase R digestion (n = 3); (e) Natural decay rates of hsa_circ_0136666 and linear PRKDC were assessed after Actinomycin D treatment (n = 3); (f) Amplification of hsa_circ_0136666 and linear PRKDC using oligo dT and random primers (n = 3); (g) FITC-based fluorescence imaging showing the localization of hsa_circ_0136666 in gastric cancer tissue sections; (h) Comparative expression analysis of hsa_circ_0136666 across different tissue types. Data are shown as mean ± SD; statistical significance was determined by Student's t-test (*P < 0.05, **P < 0.01, ***P < 0.001, ****P < 0.0001).

To verify the circular configuration, RNase R digestion assays were performed. The circular form of the RNA exhibited substantial resistance to degradation. In contrast, the linear PRKDC transcript was largely eliminated **(Figure 1d)**. Treatment with Actinomycin D further revealed that hsa_circ_0136666 displayed slower natural degradation kinetics compared to its linear parent gene **(Figure 1e)**. Additionally, amplification attempts using oligo dT primers failed to generate products for hsa_circ_0136666, consistent with the absence of a

poly(A) tail. In contrast, random primers successfully amplified it **(Figure 1f)**. Collectively, these experiments confirmed the circular architecture of hsa_circ_0136666 and demonstrated its enhanced stability relative to the linear PRKDC mRNA.

Fluorescent probe hybridization was utilized to visualize the subcellular and tissue distribution of hsa_circ_0136666, revealing broad expression across various stages of gastric cancer **(Figure 1g)**. Expression was markedly elevated in carcinoma in situ compared to normal tissues, with intermediate levels observed in adjacent paracancerous regions and metastatic lesions **(Figure 1h)**. These patterns underscore the significant involvement of hsa_circ_0136666 in gastric cancer development and progression. Analysis of clinical gastric cancer data from the TCGA database indicated that elevated miR-375 levels were associated with improved patient survival. In contrast, reduced expression trended toward poorer outcomes. Higher PRKDC expression showed a negative correlation with patient survival time.

In summary, hsa_circ_0136666 possesses a stable circular structure that confers resistance to degradation and is strongly upregulated in gastric cancer tissues. These characteristics suggest its active participation in regulatory networks that drive gastric cancer progression.

Hsa_circ_0136666 drives tumor proliferation and facilitates tumor immune escape

We observed that hsa_circ_0136666 is widely distributed across diverse gastric cancer tissue samples and is similarly detectable in multiple gastric cancer cell lines. Its expression was consistently higher in tumor-derived cell lines relative to the normal gastric epithelial cell line GES-1 **(Figure 2a)**. This indicates that hsa_circ_0136666 exhibits tissue- and disease-specific enrichment, with prominent upregulation in gastric cancer.

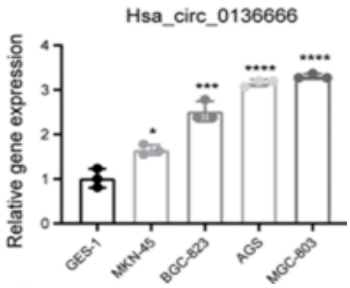

a)

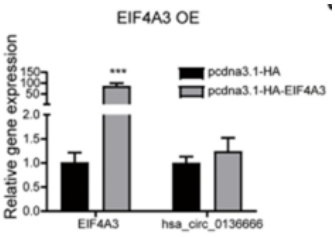

b)

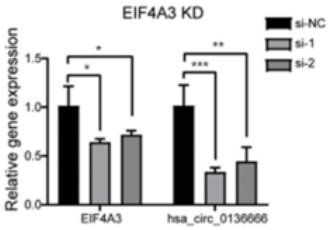

c)

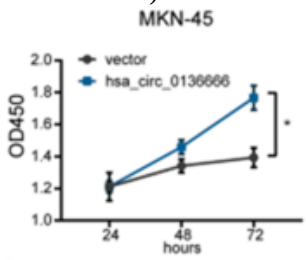

d)

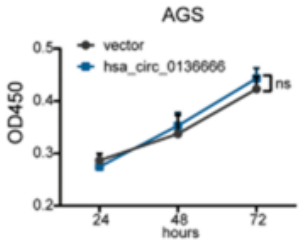

e)

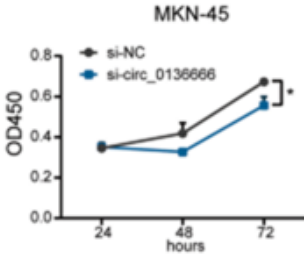

f)

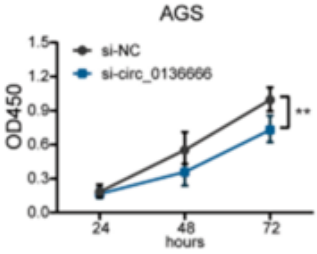

g)

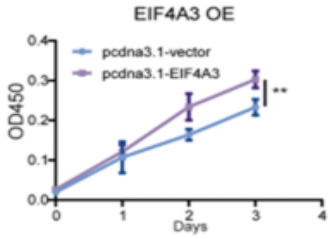

h)

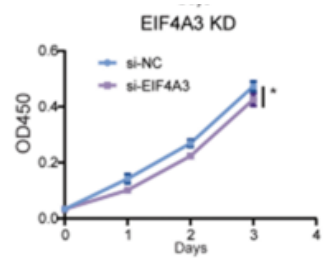

i)

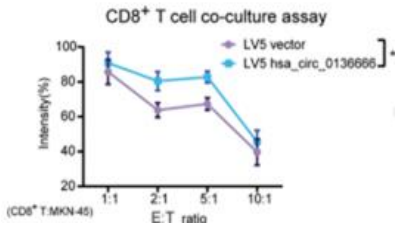

j)

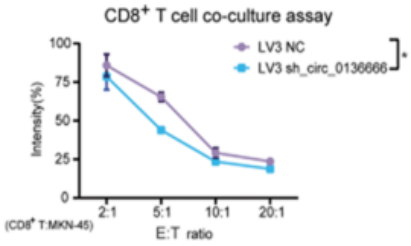

k)

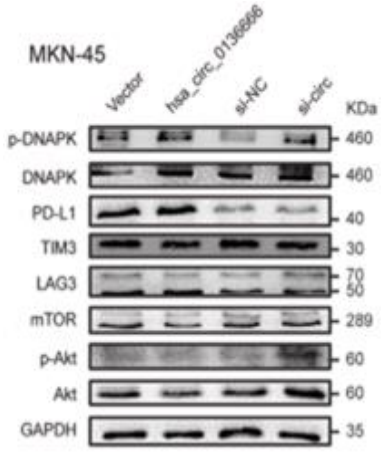

l)

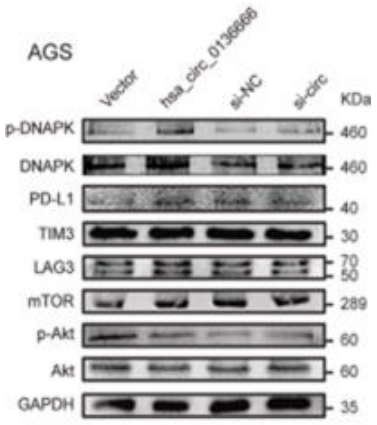

m)

Figure 2. Hsa_circ_0136666 drives tumor cell proliferation. It facilitates immune evasion

(a) Levels of hsa_circ_0136666 in multiple gastric cancer cell lines relative to the normal gastric epithelial cell line GES-1, (b) Impact of EIF4A3 overexpression on hsa_circ_0136666 abundance, (c) Impact of EIF4A3 knockdown on hsa_circ_0136666 abundance, (d) Overexpression of hsa_circ_0136666 enhanced proliferation of MKN-45 cells, (e). Overexpression of hsa_circ_0136666 enhanced proliferation of AGS cells, (f) Silencing of hsa_circ_0136666 suppressed proliferation of MKN-45 cells, (g) Silencing of hsa_circ_0136666 suppressed proliferation of AGS cells, (h) EIF4A3 overexpression promoted proliferation in MKN-45 cells, (i) EIF4A3 knockdown inhibited proliferation in MKN-45 cells, (j) Survival of tumor cells overexpressing hsa_circ_0136666 when co-cultured with CD8+ T cells (n = 6), (k) Survival of tumor cells with hsa_circ_0136666 knockdown when co-cultured with CD8+ T cells (n = 6), (l) Western blot analysis of immune checkpoint proteins and PI3K signaling pathway components in MKN-45 cells, (m) Western blot analysis of immune checkpoint proteins and PI3K signaling pathway components in AGS cells. Data are expressed as mean ± SD (n = 3 unless otherwise specified). Statistical comparisons were performed using Student's t-test (*P < 0.05, **P < 0.01, ***P < 0.001, ****P < 0.0001).

Consistent with prior reports [23], EIF4A3 serves as a key subunit of the exon junction complex and is critical for pre-mRNA splicing. It also plays a major role in regulating the back-splicing events that generate circRNAs. Analysis using the Circular RNA Interactome database (https://circinteractome.nia.nih.gov/index.html)

identified four potential EIF4A3 binding sites flanking the hsa_circ_0136666 pre-mRNA region. Subsequent qRT-PCR assays confirmed that elevating EIF4A3 levels increased hsa_circ_0136666 expression, whereas reducing EIF4A3 suppressed its expression in gastric cancer cells **(Figures 2b and 2c)**.

CCK-8 assays demonstrated that forced expression of hsa_circ_0136666 significantly accelerated cancer cell growth **(Figures 2d-2e)**, while siRNA-mediated knockdown of hsa_circ_0136666 markedly restrained proliferation **(Figures 2f-2g)**. These results highlight the critical contribution of hsa_circ_0136666 to tumor expansion. Similarly, overexpression of EIF4A3 enhanced gastric cancer cell proliferation **(Figure 2h)**, whereas its depletion inhibited proliferation **(Figure 2i)**.

Gene Ontology (Biological Process) enrichment analysis of circRNA-related genes from GSE147698 data revealed that transcripts negatively associated with miR-375 were predominantly linked to signal transduction, immune responses, and inflammatory processes. KEGG pathway analysis further highlighted enrichment in the T cell receptor signaling pathway. Previous studies have indicated that patients harboring PRKDC mutations often exhibit stronger responses to immunotherapy, suggesting that PRKDC promotes tumor aggressiveness partly by dampening immune surveillance [24].

We therefore investigated the immune-related functions of hsa_circ_0136666 in tumor progression. Given that CD8+ T cells are the primary cytotoxic effectors of cellular immunity—eliminating cancer cells by releasing perforin, granzyme B, and IFN-γ—we examined their interactions with modified tumor cells. Cancer cells overexpressing hsa_circ_0136666 displayed significantly higher survival rates when co-cultured with activated CD8+ T cells, an effect that was abrogated upon hsa_circ_0136666 knockdown **(Figures 2j-2k)**. These observations support the notion that hsa_circ_0136666 confers resistance to T cell-mediated anti-tumor immunity.

Immune checkpoint blockade, particularly targeting the CTLA4 or PD-1/PD-L1 axis, has emerged as a cornerstone of cancer immunotherapy across multiple malignancies. Reports suggest that PRKDC mutations may enhance immunotherapy sensitivity by modulating interferon-γ signaling, the PD-L1 pathway, and other immune-related pathways, and by suppressing TGF-β [25]. In line with this, we examined immune checkpoint molecules and found that hsa_circ_0136666 strongly upregulated their protein levels, most notably PD-L1 **(Figure 2l)**. Conversely, siRNA-mediated knockdown of hsa_circ_0136666 reduced PD-L1 protein expression **(Figure 2m)**. Notably, hsa_circ_0136666 exerted minimal influence on the mRNA levels of these checkpoint genes, and its depletion tended to lower mRNA expression, indicating that its regulatory effects on immunity likely occur at the post-transcriptional or protein level rather than through direct transcriptional control.

Taken together, hsa_circ_0136666 robustly enhances gastric cancer cell proliferation in vitro while simultaneously protecting tumor cells from immune recognition and attack. Its own biogenesis is under the control of EIF4A3.

Hsa_circ_0136666 modulates anti-tumor immunity to promote immune escape

To evaluate in vivo effects, we established a syngeneic tumor transplantation model using murine gastric cancer cells. C57BL/6 mice bearing MFC tumors overexpressing hsa_circ_0136666 exhibited accelerated tumor growth **(Figure 3a)** and increased tumor weights **(Figures 3b and 3c)**. Comparable results were obtained in the BALB/c nude mouse xenograft model. These data indicate that human hsa_circ_0136666 promotes aggressive tumor progression in vivo.

The tumor immune microenvironment often acts as a barrier to effective anti-cancer therapies, involving various immunosuppressive cell populations and soluble factors. We therefore assessed whether hsa_circ_0136666 influences immune cell recruitment and composition within the tumor microenvironment (TME), with particular attention to effector T cells, regulatory T cells (Tregs), M2-like macrophages, and myeloid-derived suppressor cells (MDSCs). Overexpression of hsa_circ_0136666 led to a substantial reduction in overall tumor-infiltrating T cells and promoted polarization of tumor-associated macrophages toward the pro-tumorigenic M2 phenotype **(Figures 3d and 3e)**. Additionally, there was a notable expansion of both MDSC and Treg populations in tumors overexpressing hsa_circ_0136666 **(Figures 3f and 3g)**.

Validation experiments confirmed stable overexpression of hsa_circ_0136666 in the MFC cell model **(Figure 3h)**. Collectively, these findings demonstrate that hsa_circ_0136666 fosters a tumor-promoting, immunosuppressive milieu that drives malignant progression.

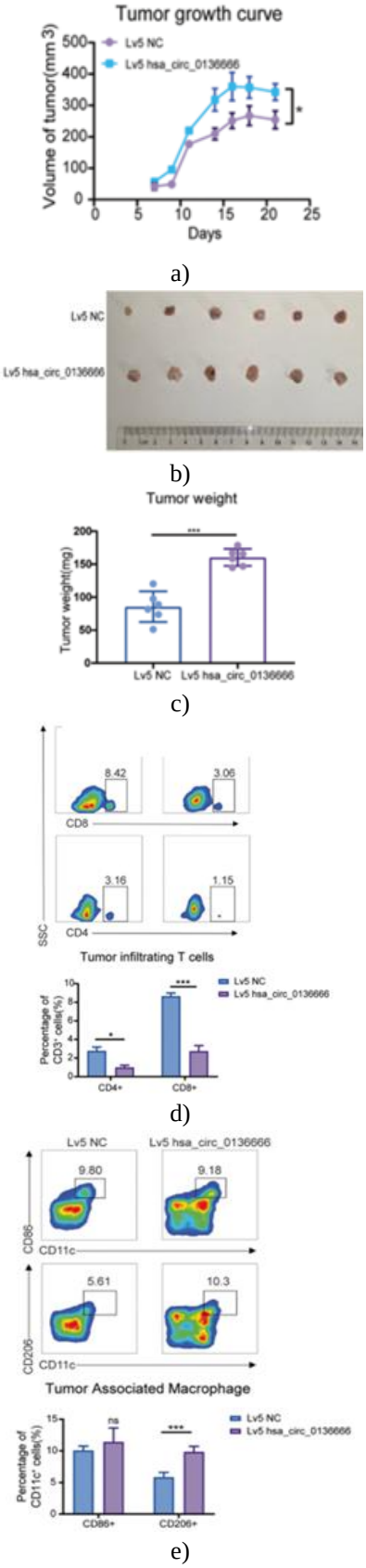

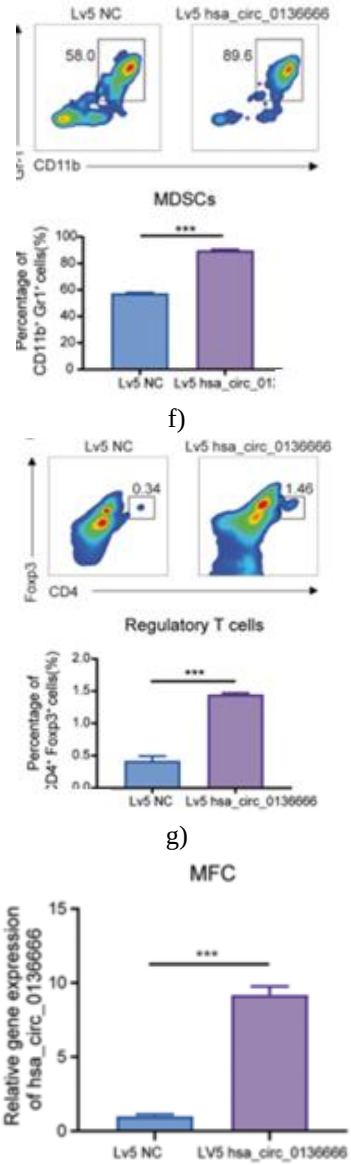

Figure 3. Hsa_circ_0136666 modulates anti-tumor immune responses to promote immune evasion

(a) Tumor growth curves in mice bearing tumors from Lv5 MFC cells, (b) Representative photographs of excised tumors from mice, (c) Quantitative comparison of tumor weights in mice, (d) Changes in the proportion of tumor-infiltrating T lymphocytes, (e) Changes in the proportion of tumor-associated macrophages, (f) Changes in the proportion of tumor-infiltrating MDSC cells, (g) Changes in the proportion of tumor-infiltrating regulatory T cells. Data are shown as mean ± SD (n = 6). Statistical analysis was performed using Student's t-test (*P < 0.05, ***P < 0.001). (h) Confirmation of

hsa_circ_0136666 overexpression in MFC cells (***P < 0.001).

Earlier research has established that cytokines are crucial regulators of cellular immunity. For instance, TGF-β remodels the tumor microenvironment and attenuates anti-tumor immune responses by restricting T cell infiltration [26]. Treatment with PD-1 monoclonal antibodies can trigger IFN-γ-mediated YAP aggregation in tumor cells, which in turn activates a transcriptional network of immunosuppressive genes and contributes to adaptive resistance [27]. The IL-6/STAT3 signaling axis is known to expand immunosuppressive cell populations and disrupt T cell subset balance [28]; moreover, inhibiting IL-6 has been shown to potentiate the therapeutic efficacy of anti-PD-L1 agents [20].

In our experiments, tumor tissues overexpressing hsa_circ_0136666 displayed elevated levels of IFN-γ and IL-6, with no notable alteration in TGF-β. In contrast, tissues with hsa_circ_0136666 knockdown exhibited a downward trend in these pro-tumorigenic cytokines. Immunohistochemical staining of tumor sections further revealed more pronounced pathological deterioration and increased PD-L1 protein expression in the presence of hsa_circ_0136666 overexpression. Overall, these results demonstrate that hsa_circ_0136666 accelerates tumor growth and actively shapes an immunosuppressive microenvironment in vivo.

Hsa_circ_0136666 controls gastric cancer progression by sponging miR-375

Our prior investigations established that miR-375 suppresses gastric carcinogenesis associated with *H. pylori* infection. *H. pylori* itself can downregulate miR-375, thereby influencing inflammatory cytokine production and immune cell differentiation in the gastric mucosa. Consistent with our earlier predictions, hsa_circ_0136666 expression showed a strong negative correlation with miR-375 levels **(Figure 4a)**.

Potential binding sites between hsa_circ_0136666 and miR-375 were identified using the starBase v2.0 online platform (http://starbase.sysu.edu.cn/starbase2) **(Figure 4b)**. RNA immunoprecipitation (RIP) assays confirmed their direct interaction: Argonaute 2 (AGO2), a core component of the RNA-induced silencing complex (RISC), effectively pulled down miR-375 when associated with wild-type hsa_circ_0136666 **(Figure 4c)**. Complementary dual-luciferase reporter assays further validated this binding. Co-transfection of miR-375 with the wild-type hsa_circ_0136666 reporter construct significantly reduced luciferase activity, whereas mutation of the predicted binding site abolished this repressive effect **(Figure 4d)**.

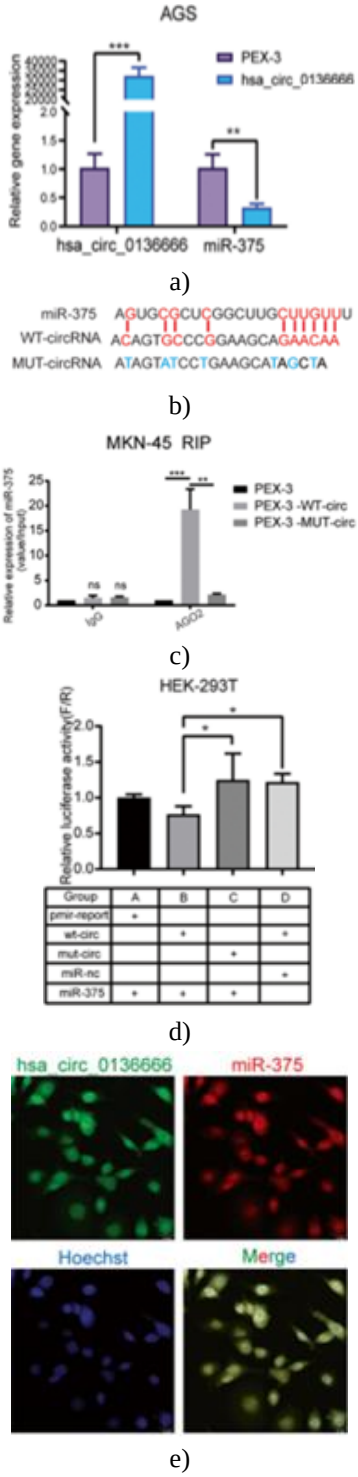

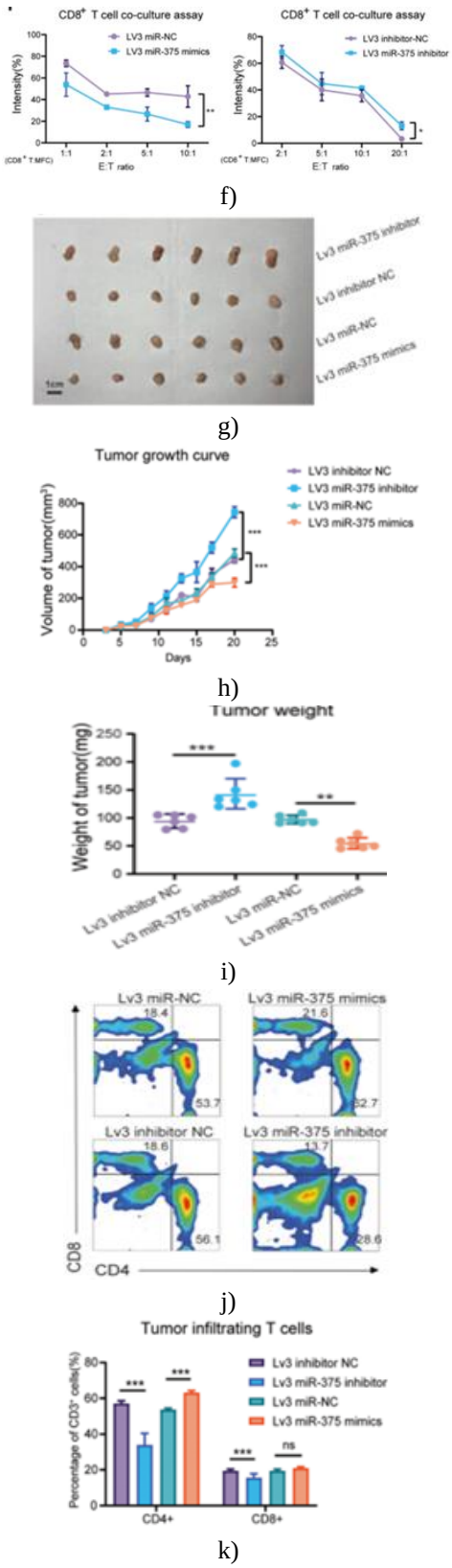

Figure 4. Hsa_circ_0136666 promotes gastric cancer progression by acting as a sponge for miR-375

(a) Negative correlation between the relative expression levels of hsa_circ_0136666 and miR-375 (n = 3), (b). Complementary base-pairing sites between miR-375 and wild-type hsa_circ_0136666, (c). RIP assay confirming the sponging activity of hsa_circ_0136666 (n = 3), (d) Dual-luciferase reporter assay validating the direct interaction between hsa_circ_0136666 and miR-375 (n = 6), (e) RNA fluorescence in situ hybridization demonstrating colocalization of hsa_circ_0136666 and miR-375, (f) Survival rates of tumor cells with hsa_circ_0136666 overexpression or knockdown when co-cultured with CD8+ T cells (n = 6), (g) Representative images of tumors from Lv3 miR-375 tumor-bearing mice, (h) Tumor growth curves in Lv3 miR-375 tumor-bearing mice (n = 6), (i) Comparison of tumor weights across groups (n = 6), (j) Differences in tumor-infiltrating T lymphocyte distribution among Lv3 tumor-bearing mouse groups (n = 6), (k) Quantitative analysis of tumor-infiltrating T lymphocytes across different groups (n = 6). Data are presented as mean ± SD. Statistical significance was assessed by Student's t-test (*P < 0.05, **P < 0.01, ***P < 0.001).

To determine whether hsa_circ_0136666 exerts its oncogenic effects primarily through sponging miR-375, we performed RNA fluorescence in situ hybridization. This revealed that hsa_circ_0136666 is predominantly cytoplasmic and exhibits a distribution pattern nearly identical to that of miR-375 **(Figure 4e)**.

Furthermore, miR-375 itself was found to influence tumor immunity. Cancer cells transfected with miR-375 mimics displayed reduced survival when co-cultured with activated CD8+ T cells, whereas cells transfected with miR-375 inhibitors showed enhanced survival **(Figure 4f)**. In vivo validation using C57BL/6 tumor-bearing mice confirmed the tumor-suppressive role of miR-375 **(Figure 4g)**. Overexpression of miR-375 significantly slowed tumor growth and decreased tumor weight. At the same time, miR-375 inhibition accelerated tumor progression and increased tumor burden **(Figures 4h and 4i)**.

Examination of T cell populations within the tumor microenvironment showed that miR-375 overexpression markedly enhanced T cell infiltration and proliferation, with increases observed in both CD4+ and CD8+ T cell subsets **(Figure 4j)**. This effect was reversed in the miR-375 inhibitor group, where T cell expansion was suppressed **(Figure 4k)**. These findings collectively indicate that hsa_circ_0136666 functions as a molecular sponge for miR-375, thereby preventing miR-375 from

exerting its physiological tumor-suppressive and immune-enhancing activities.

Hsa_circ_0136666 governs immune responses via the miR-375/PRKDC signaling axis

MicroRNAs typically bind to the 3' untranslated regions (3'UTRs) of target mRNAs, leading to their degradation or translational repression. To identify targets of miR-375, we re-analyzed the GSE147698 dataset and detected 1,777 upregulated and 262 downregulated mRNAs in cells overexpressing miR-375 **(Figure 5a)**. Notably, the parental gene PRKDC emerged as a potential direct target of miR-375.

Bioinformatics analysis using the starBase database (starbase.sysu.edu.cn) identified complementary pairing sequences between miR-375 and the 3'UTR of PRKDC **(Figure 5b)**. qRT-PCR experiments demonstrated a close positive association between hsa_circ_0136666 and its host gene PRKDC: overexpression of hsa_circ_0136666 increased PRKDC levels, while its knockdown decreased PRKDC expression. Additionally, a significant negative correlation was observed between miR-375 and PRKDC mRNA levels.

Direct binding was further confirmed through RIP assays and dual-luciferase reporter experiments **(Figures 5c and 5d)**.

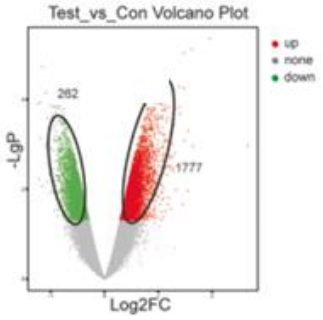

a)

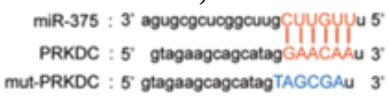

b)

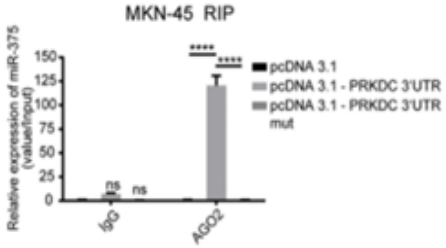

c)

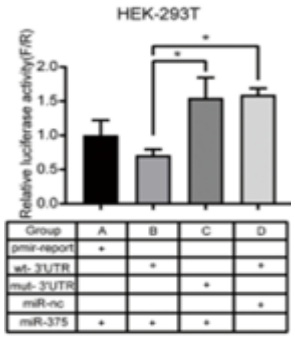

d)

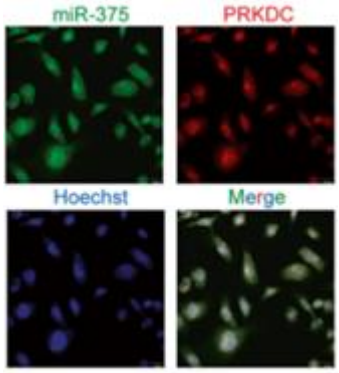

e)

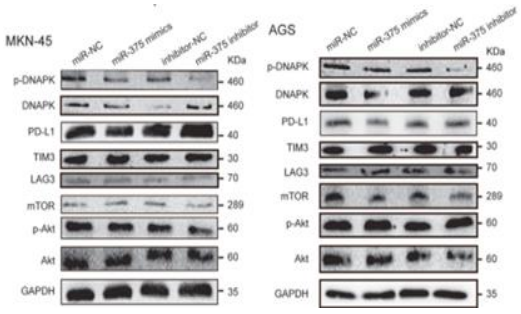

f)

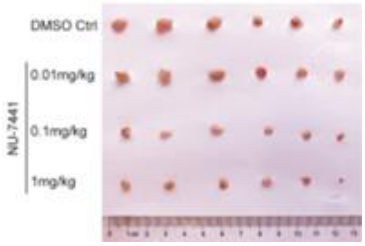

g)

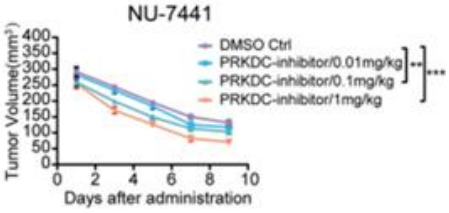

h)

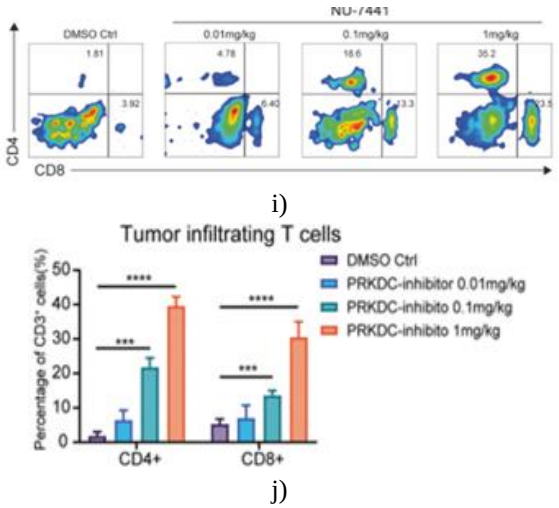

Figure 5. Hsa_circ_0136666 controls immune responses via the miR-375/PRKDC signaling pathway

(a) Microarray analysis of cells overexpressing miR-375 identified 1,777 upregulated genes and 262 downregulated genes, (b) Complementary base-pairing sites between miR-375 and the wild-type 3'UTR of PRKDC mRNA, (c) RIP assay confirming the interaction between miR-375 and PRKDC (n = 3), (d) Dual-luciferase reporter assay verifying the binding between the PRKDC 3'UTR and miR-375 (n = 6), (e) RNA in situ hybridization demonstrating colocalization of PRKDC mRNA 3'UTR with miR-375, (f) Western blot analysis of immune checkpoint proteins and PI3K signaling pathway components in MKN-45 cells following miR-375 overexpression, (g) Representative photographs of tumors from tumor-bearing mice treated with NU-7441, (h) Tumor growth curves of tumor-bearing mice under NU-7441 treatment (n = 6), (i) Differences in tumor-infiltrating T lymphocyte distribution across treatment groups in tumor-bearing mice under NU-7441 (n = 6), (j) Quantitative analysis of tumor-infiltrating T lymphocytes across different groups (n = 6). Data are presented as mean ± SD. Statistical significance was determined using Student's t-test (*P < 0.05, **P < 0.01, ***P < 0.001, ****P < 0.0001).

We observed that PRKDC mRNA is primarily localized in the cytoplasm, displaying a distribution pattern nearly identical to that of miR-375 **(Figure 5e)**. Through incorporation into the RISC complex, miRNAs bind to the 3'UTR of target mRNAs, thereby inhibiting their translation. In this context, miR-375 directly regulates the protein product of PRKDC, known as DNA-PKcs—the catalytic subunit of DNA-dependent protein kinase (DNA-PK). DNA-PK functions together with the Ku70/Ku80 heterodimer in the repair of DNA double-strand breaks and recombination processes.

Following transfection of miR-375 mimics or inhibitors into MKN-45 and AGS cells, total protein levels were assessed. miR-375 overexpression led to downregulation of PRKDC and subsequent reduction in DNA-PK protein levels **(Figure 5f)**. Autophosphorylation serves as a marker of DNA-PK activation, with phosphorylation levels reflecting its enzymatic activity. Although an increase in p-DNAPK was observed with hsa_circ_0136666 overexpression, the change did not reach statistical significance. As DNA-PK belongs to the PI3K-related kinase family, we examined downstream effects and found that DNA-PK downregulation did not significantly affect Akt or p-Akt levels. These results suggest that the upregulation of DNA-PK by hsa_circ_0136666 has a limited effect on the Akt/mTOR pathway and that hsa_circ_0136666 likely promotes oncogenesis through mechanisms independent of Akt/mTOR signaling.

Inhibition of DNA-PK activity produced robust anti-tumor effects. Treatment with high concentrations of NU-7441, a selective DNA-PK inhibitor, resulted in strong tumor suppression **(Figures 5g and 5h)**. This treatment also led to markedly enhanced T cell recruitment into the tumor compared to controls **(Figure 5i)**, thereby activating immune responses and promoting effective cancer cell elimination **(Figure 5j)**. Overall, these data indicate that hsa_circ_0136666 acts as a sponge for miR-375, preventing miRNA-mediated degradation of target genes. This allows DNA-PK to exert its pro-tumorigenic functions, ultimately contributing to immune escape.

Protein kinase DNA-PK induces dual-site phosphorylation of PD-L1 at T20 and T22 to promote protein stabilization

Previous experiments revealed a close link between PRKDC and the immune checkpoint molecule PD-L1. We therefore hypothesized that DNA-PK may directly interact with and phosphorylate PD-L1, thereby enhancing its stability, increasing its accumulation, and facilitating tumor immune evasion. To test this, endogenous co-immunoprecipitation was performed in tumor cells. PD-L1 was successfully pulled down using an anti-DNA-PK antibody, and reciprocally, DNA-PK

was pulled down with an anti-PD-L1 antibody **(Figure 6a)**.

In HEK-293T cells transfected with hsa_circ_0136666 or miR-375 mimics, pull-down efficiency increased substantially in parallel with elevated DNA-PK levels **(Figures 6b and 6c)**. Immunofluorescence staining further demonstrated clear colocalization of DNA-PK and PD-L1 in the cytoplasm **(Figure 6d)**.

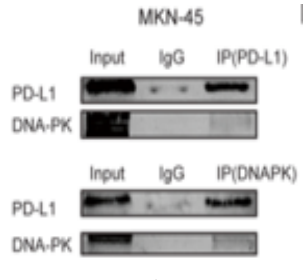

a)

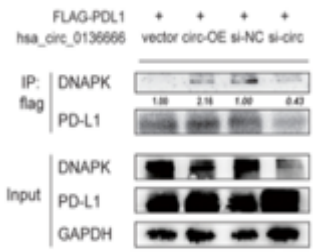

b)

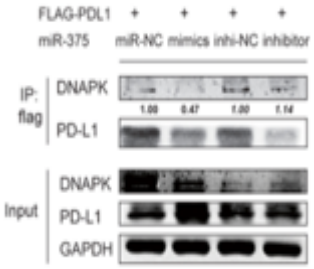

c)

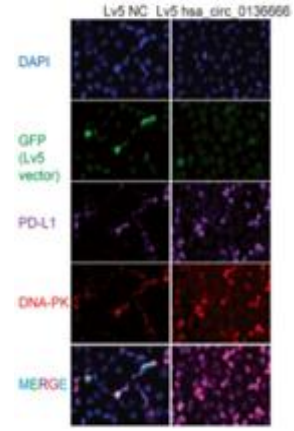

d)

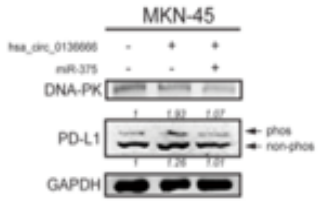

e)

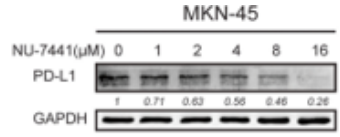

f)

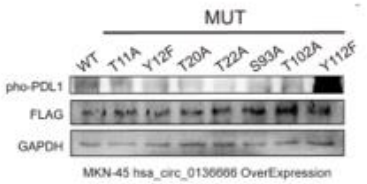

g)

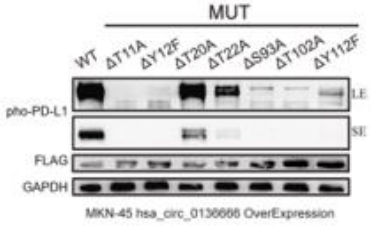

h)

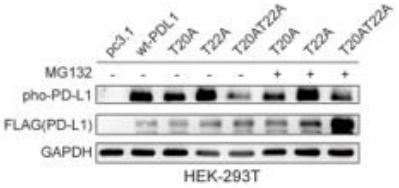

i)

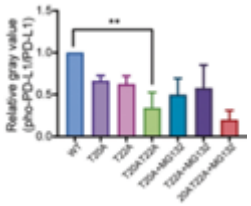

j)

k)

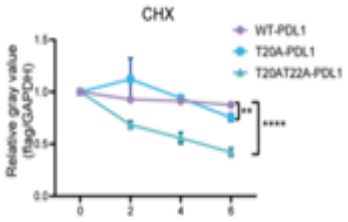

l)

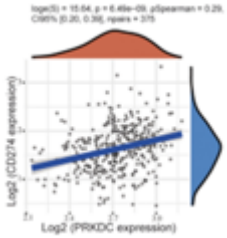

m)

Figure 6. Protein kinase DNA-PK induces dual-site phosphorylation of PD-L1 at T20 and T22 to enhance protein stability

(a) Endogenous co-immunoprecipitation confirming the interaction between DNA-PK and PD-L1, (b) Exogenous co-immunoprecipitation validating the binding of DNA-PK and PD-L1 in 293T cells upon hsa_circ_0136666 overexpression, (c) Exogenous co-immunoprecipitation validating the binding of DNA-PK and PD-L1 in 293T cells in the presence of miR-375, (d) Immunofluorescence staining demonstrating colocalization of DNA-PK and PD-L1, (e) Rescue experiment using phos-tag acrylamide SDS-PAGE to detect phosphorylated PD-L1, (f) The PRKDC inhibitor NU-7441 reduced PD-L1 protein levels in a concentration-dependent manner, (g) Detection of phosphorylated PD-L1 following single-site mutations at seven potential phosphosites, (h) Detection of phosphorylated PD-L1 following multiple-site mutations, (i) Detection of phosphorylated PD-L1 after double-site mutation under MG-132 treatment, (j) Quantification of phospho-PD-L1 levels after dual phosphorylation site mutation (n = 3), (k) CHX chase assay assessing PD-L1 protein stability, (l) Quantitative analysis of PD-L1 protein stability (n = 3), (m) TCGA database analysis of the correlation between CD274 (PD-L1) and PRKDC expression across 375 gastric cancer samples. Data are presented as mean ± SD. Statistical significance was evaluated by Student's t-test (**P < 0.01, ****P < 0.0001).

Given that DNA-PK is a member of the PI3K kinase superfamily, we investigated whether PRKDC directly phosphorylates PD-L1. Rescue experiments demonstrated that hsa_circ_0136666 overexpression increased PD-L1 phosphorylation, an effect partially reversed by miR-375 **(Figure 6e)**. Treatment with NU-7441, which inhibits DNA-PK activity, also suppressed PD-L1 protein expression **(Figure 6f)**.

After confirming direct binding between DNA-PK and PD-L1, we sought to identify specific phosphorylation sites. Mass spectrometry analysis following DNA-PK immunoprecipitation in HEK-293T cells revealed seven candidate phosphorylation sites on PD-L1. To pinpoint the sites targeted by DNA-PK, we generated mutants at these seven positions. We analyzed phosphorylated proteins using phos-tag acrylamide gels. Two sites, T20 and T22, showed significantly reduced phosphorylation levels when mutated **(Figure 6g)**. In contrast, maintaining only one of these sites intact while mutating the others resulted in elevated phosphorylated protein levels **(Figure 6h)**.

The double mutant (T20A/T22A) caused a more pronounced decrease in PD-L1 phosphorylation compared to single-site mutations in MKN-45 cells overexpressing hsa_circ_0136666 **(Figures 6i and 6j)**. Additionally, the double-mutant PD-L1 protein exhibited reduced stability and underwent faster degradation within 6 hours under cycloheximide (CHX) treatment compared to wild-type PD-L1 **(Figures 6k and 6l)**. Analysis of clinical data from the TCGA database further supported a strong positive correlation between DNA-PK (PRKDC) and PD-L1 (CD274) expression in gastric adenocarcinoma samples **(Figure 6m)**.

In summary, DNA-PK directly binds to and colocalizes with PD-L1. It phosphorylates PD-L1 at the dual T20/T22 sites, protecting it from degradation, increasing its stability and accumulation, and thereby promoting immune dysregulation.

Hsa_circ_0136666 represents a novel therapeutic target; siRNA delivery enhances anti-PD-L1 treatment efficacy

To evaluate the potential of hsa_circ_0136666 as a druggable target, we established a subcutaneous tumor model in C57BL/6 mice **(Figure 7a)**. MFC cells overexpressing hsa_circ_0136666 were implanted, and tumor-bearing mice were randomly assigned to four treatment groups. Nanoliposome-encapsulated siRNA (LNP-siRNA) was administered intratumorally (equivalent to 40 μg siRNA per mouse in 100 μl

volume). The siRNA achieved approximately 50% knockdown efficiency at the cellular level **(Figure 7b)**. Mice also received intraperitoneal injections of anti-mouse PD-L1 monoclonal antibody (2 mg/kg), with both treatments administered every three days. Compared to the saline and LNP-siNC control groups, tumor growth was markedly suppressed in the LNP-siRNA group. The combination of LNP-siRNA and anti-PD-L1 produced even greater inhibition than anti-PD-L1 monotherapy, resulting in the smallest tumor volumes and weights among all groups. The combination therapy achieved an inhibition rate of approximately 50–60% relative to controls, as measured by tumor size and weight **(Figures 7c-7f)**. Body weights remained comparable across the four groups, indicating that the treatments were well tolerated without obvious toxicity **(Figure 7d)**. Intratumoral injection allowed efficient delivery of siRNA directly to the tumor site, while the nanoliposome formulation protected the siRNA from nuclease degradation in circulation.

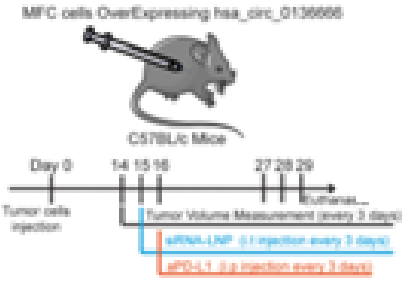

a)

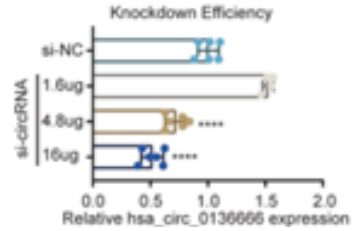

b)

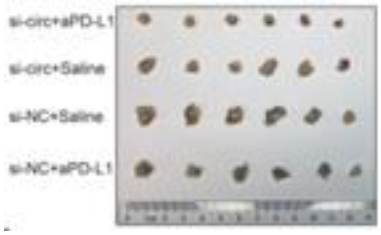

c)

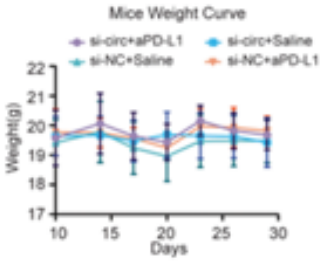

d)

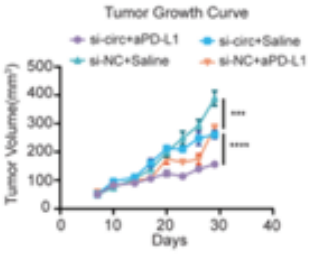

e)

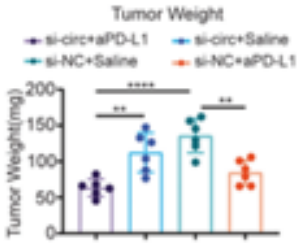

f)

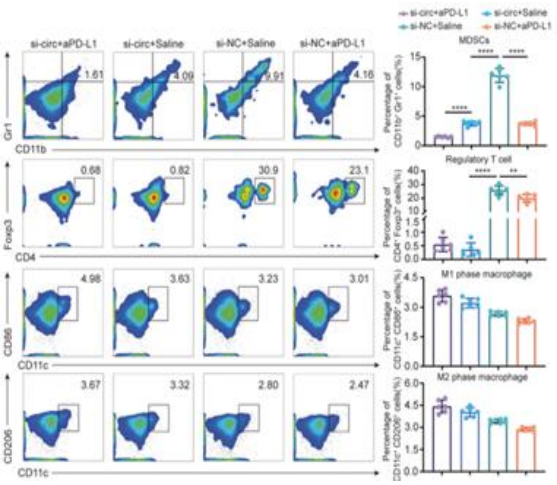

g)

Figure 7. Hsa_circ_0136666 serves as a novel therapeutic target, with siRNA delivery significantly enhancing anti-PD-L1 therapeutic efficacy

(a) Schematic illustration of the animal treatment regimen. Fourteen days after tumor cell inoculation, mice received intratumoral injections of LNP-siRNA at 2 mg/kg, followed by intraperitoneal administration of 2

mg/kg anti-mouse PD-L1 inhibitor the next day. Treatments were given every three days for a total of five cycles, (b) qRT-PCR analysis of siRNA knockdown efficiency (n = 3), (c) Representative photographs of tumors from tumor-bearing mice receiving LNP-siRNA and inhibitor treatments, (d) Body weight curves of tumor-bearing mice (n = 6), (e) Tumor growth curves of tumor-bearing mice (n = 6), (f) Comparison of tumor weights across groups (n = 6), (g) Differences and quantitative analysis of immunosuppressive cell populations in the tumor regions among treatment groups (n = 6). **P < 0.01, ***P < 0.001, ****P < 0.0001.

Consistent with initial expectations, siRNA treatment alone partially restrained tumor growth, though the effect was less pronounced than anti-PD-L1 monoclonal antibody (mAb) monotherapy. Importantly, LNP-siRNA demonstrated substantial benefits in remodeling the tumor microenvironment, particularly by altering the proportions of immunosuppressive cells. Treatment with LNP-siRNA led to marked suppression of MDSCs within the tumor, with the LNP-siRNA plus anti-PD-L1 combination group showing the lowest MDSC levels. Similarly, tumor-infiltrating regulatory T cells were significantly reduced in all LNP-siRNA-treated groups compared to those without siRNA. In contrast, tumor-associated macrophages showed no significant alterations across treatments **(Figure 7g)**.

We further examined effector CD8+ T cells and their granzyme B release in the tumor area. Immunofluorescence staining of tumor sections revealed that the LNP-siRNA combined with anti-PD-L1 group exhibited the most extensive infiltration of CD8+ T cells, the highest granzyme B expression, and the lowest PD-L1 levels. Both the LNP-siRNA monotherapy and anti-PD-L1 monotherapy groups showed reduced PD-L1 expression compared with the negative control group.

Collectively, these findings indicate that LNP-siRNA effectively augments the anti-tumor efficacy of anti-PD-L1 agents and strongly impedes the recruitment and accumulation of immunosuppressive cells. The approach showed no discernible toxicity or adverse effects on body weight, supporting its potential safety for further in vivo applications.

In recent years, circRNAs have been recognized as a major class of non-coding RNAs that play diverse regulatory roles in cancer development and progression. Although some circRNAs can encode novel short peptides that influence cancer biology, we did not explore this possibility for hsa_circ_0136666. To our knowledge, this circRNA lacks a ribosome binding site (IRES element) and contains no ATG start codon within its circular structure. These features indicate that hsa_circ_0136666 is unlikely to possess protein-coding potential or generate micro-peptides.

The present study primarily focused on the miRNA-sponging function of hsa_circ_0136666, a prominent and actively researched mechanism in recent circRNA literature. Numerous reports have documented that circRNAs influence tumor growth via miRNA sponging; however, most of these investigations focus on direct effects on cancer cell proliferation, invasion, and migration, with relatively few addressing the immunological roles of circRNAs.A central discovery of this work is that hsa_circ_0136666 acts as a sponge for miR-375, thereby counteracting miR-375-mediated gene silencing and preventing PRKDC downregulation. The resulting increase in DNA-PK protein levels promotes its interaction with PD-L1, leading to PD-L1 phosphorylation, enhanced protein stability, and abnormal membrane clustering. These molecular events ultimately drive tumor immune escape **(Figure 8)**.

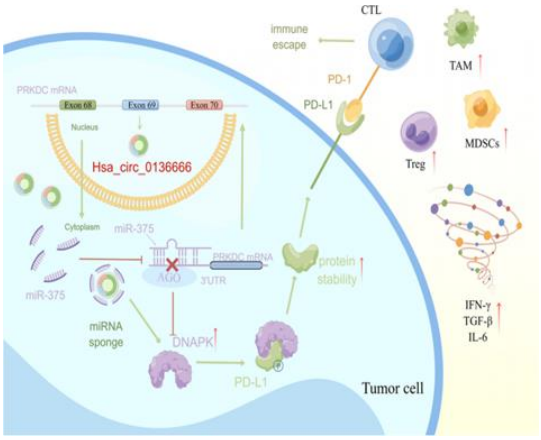

Figure 8. Signal transduction pathway diagram of hsa_circ_0136666 in promoting gastric cancer progression.

Specifically, the hsa_circ_0136666/miR-375/PRKDC axis elevates DNA-PK protein expression, which, in turn, drives PD-L1 phosphorylation. The resulting enhancement in PD-L1 stability leads to abnormal clustering at the tumor cell membrane, ultimately triggering immune escape.

Small nucleic acid drugs, also known as RNA interference (RNAi) therapeutics, represent a distinct category of medicines, distinct from traditional small-molecule compounds and antibody-based therapies.

These agents consist of specific nucleotide sequences that target mRNA, induce gene silencing, and thereby suppress the expression of disease-related proteins, thereby achieving therapeutic effects [29]. This class encompasses siRNAs, miRNAs, antisense oligonucleotides, and related molecules. The foundational discoveries underlying RNAi technology were recognized with the Nobel Prize in Physiology or Medicine in 2006, marking a major milestone in biomedical science [30-33].

In principle, RNAi-based approaches can be applied to any condition involving aberrant overexpression of specific genes, including viral infections, cancers, and inflammatory disorders. Consequently, investigating the roles and molecular mechanisms of small nucleic acid drugs in oncology constitutes a vital direction for developing innovative biotechnological therapies for gastric cancer. Such research offers fresh perspectives for identifying drug targets, advancing clinical diagnostics, and improving treatment strategies. Lipid nanoparticles (LNPs) provide an effective delivery platform that addresses key challenges in siRNA transport, while also improving the overall efficacy and biocompatibility of nucleic acid-based medicines.

The in vivo gene-silencing efficiency of unmodified ("naked") siRNA is extremely low. Naked siRNA is rapidly degraded by serum nucleases and quickly cleared by the kidneys. Additionally, its large size and strong negative charge impede passage across cell membranes, limiting intracellular delivery. Therefore, robust delivery systems are essential for directing siRNA to target cells and tissues. Liposomes, composed of phospholipid bilayers, offer excellent biocompatibility and serve as versatile drug carriers that enhance transdermal absorption and intracellular uptake of therapeutic payloads.

Conclusion

Our study has several limitations. First, although we focused on hsa_circ_0136666 because its host gene participates in a regulatory feedback loop, other differentially expressed circRNAs identified in the analysis were not examined. Second, we did not explore additional potential functions of hsa_circ_0136666, such as interactions with RNA-binding proteins. Mechanisms beyond miR-375 sponging may contribute to its effects on tumor proliferation and immune evasion. Third, regarding therapeutic applications, LNP-siRNA monotherapy produced only modest tumor inhibition. While the combination with PD-L1 inhibitors showed improved efficacy, both agents ultimately converge on the PD-L1 pathway, potentially limiting the potential for synergy. Further studies, including humanized mouse models and combinations with additional therapeutic agents, will be necessary to comprehensively evaluate the clinical utility of this siRNA approach.

Acknowledgments: None

Conflict of Interest: None

Financial Support: None

Ethics Statement: None

References

1. Bray F, Ferlay J, Soerjomataram I, Siegel RL, Torre LA, Jemal A. Global cancer statistics 2018: GLOBOCAN estimates of incidence and mortality worldwide for 36 cancers in 185 countries. CA Cancer J Clin. 2018;68(6):394-424.
2. Chen W, Sun K, Zheng R, Zeng H, Zhang S, Xia C, et al. Cancer incidence and mortality in China, 2014. Chin J Cancer Res. 2018;30(1):1-12.
3. Hallinan JT, Venkatesh SK. Gastric carcinoma: imaging diagnosis, staging and assessment of treatment response. Cancer Imaging. 2013;13(2):212-27.
4. Alsina M, Arrazubi V, Diez M, Tabernero J. Current developments in gastric cancer: from molecular profiling to treatment strategy. Nat Rev Gastroenterol Hepatol. 2023;20(3):155-70.
5. Zhang XO, Dong R, Zhang Y, Zhang JL, Luo Z, Zhang J, et al. Diverse alternative back-splicing and alternative splicing landscape of circular RNAs. Genome Res. 2016;26(9):1277-87.
6. Memczak S, Jens M, Elefsinioti A, Torti F, Krueger J, Rybak A, et al. Circular RNAs are a large class of animal RNAs with regulatory potency. Nature. 2013;495(7441):333-8.
7. Kristensen LS, Andersen MS, Stagsted LVW, Ebbesen KK, Hansen TB, Kjems J. The biogenesis, biology and characterization of circular RNAs. Nat Rev Genet. 2019;20(11):675-91.
8. Weng W, Wei Q, Toden S, Yoshida K, Nagasaka T, Fujiwara T, et al. Circular RNA ciRS-7—A

Promising Prognostic Biomarker and a Potential Therapeutic Target in Colorectal Cancer. Clin Cancer Res. 2017;23(14):3918-28.
9. Verduci L, Ferraiuolo M, Sacconi A, Ganci F, Vitale J, Colombo T, et al. The oncogenic role of circPVT1 in head and neck squamous cell carcinoma is mediated through the mutant p53/YAP/TEAD transcription-competent complex. Genome Biol. 2017;18(1):237.
10. Zhang J, Liu H, Hou L, Wang G, Zhang R, Huang Y, et al. Circular RNA_LARP4 inhibits cell proliferation and invasion of gastric cancer by sponging miR-424-5p and regulating LATS1 expression. Mol Cancer. 2017;16(1):151.
11. Tang W, Fu K, Sun H, Rong D, Wang H, Cao H. CircRNA microarray profiling identifies a novel circulating biomarker for detection of gastric cancer. Mol Cancer. 2018;17(1):137.
12. Thomson DW, Dinger ME. Endogenous microRNA sponges: evidence and controversy. Nat Rev Genet. 2016;17(5):272-83.
13. Saliminejad K, Khorram Khorshid HR, Soleymani Fard S, Ghaffari SH. An overview of microRNAs: Biology, functions, therapeutics, and analysis methods. J Cell Physiol. 2019;234(5):5451-65.
14. Ni H, Qin H, Sun C, Liu Y, Ruan G, Guo Q, et al. MiR-375 reduces the stemness of gastric cancer cells through triggering ferroptosis. Stem Cell Res Ther. 2021;12(1):325.
15. Zhang Z, Chen S, Fan M, Ruan G, Xi T, Zheng L, et al. Helicobacter pylori induces gastric cancer via down-regulating miR-375 to inhibit dendritic cell maturation. Helicobacter. 2021;26(3):e12813.
16. Abdel-Wahab R, Yap TA, Madison R, Pant S, Cooke M, Wang K, et al. Genomic profiling reveals high frequency of DNA repair genetic aberrations in gallbladder cancer. Sci Rep. 2020;10(1):22087.
17. Liiv I, Rebane A, Org T, Saare M, Maslovskaja J, Kisand K, et al. DNA-PK contributes to the phosphorylation of AIRE: importance in transcriptional activity. Biochim Biophys Acta. 2008;1783(1):74-83.
18. Wang Y, Sun Q, Mu N, Sun X, Wang Y, Fan S, et al. The deubiquitinase USP22 regulates PD-L1 degradation in human cancer cells. Cell Commun Signal. 2020;18(1):112.
19. Yao H, Lan J, Li C, Shi H, Brosseau JP, Wang H, et al. Inhibiting PD-L1 palmitoylation enhances T-cell immune responses against tumours. Nat Biomed Eng. 2019;3(4):306-17.
20. Chan LC, Li CW, Xia W, Hsu JM, Lee HH, Cha JH, et al. IL-6/JAK1 pathway drives PD-L1 Y112 phosphorylation to promote cancer immune evasion. J Clin Invest. 2019;129(8):3324-38.
21. Wang X, Teng F, Kong L, Yu J. PD-L1 expression in human cancers and its association with clinical outcomes. Onco Targets Ther. 2016;9:5023-39.
22. Wu B, Song M, Dong Q, Xiang G, Li J, Ma X, et al. UBR5 promotes tumor immune evasion through enhancing IFN-gamma-induced PDL1 transcription in triple negative breast cancer. Theranostics. 2022;12(11):5086-102.
23. Liu Y, Ma L, Hua F, Min Z, Zhan Y, Zhang W, et al. Exosomal circCARM1 from spheroids reprograms cell metabolism by regulating PFKFB2 in breast cancer. Oncogene. 2022;41(14):2012-25.
24. Tan KT, Yeh CN, Chang YC, Cheng JH, Fang WL, Yeh YC, et al. PRKDC: new biomarker and drug target for checkpoint blockade immunotherapy. J Immunother Cancer. 2020;8(1):e000485.
25. Sun X, Liu T, Zhao J, Xia H, Xie J, Guo Y, et al. DNA-PK deficiency potentiates cGAS-mediated antiviral innate immunity. Nat Commun. 2020;11(1):6182.
26. Mariathasan S, Turley SJ, Nickles D, Castiglioni A, Yuen K, Wang Y, et al. TGFbeta attenuates tumour response to PD-L1 blockade by contributing to exclusion of T cells. Nature. 2018;554(7693):544-8.
27. Yu M, Peng Z, Qin M, Liu Y, Wang J, Zhang C, et al. Interferon-gamma induces tumor resistance to anti-PD-1 immunotherapy by promoting YAP phase separation. Mol Cell. 2021;81(6):1216-1230.e9.
28. Mace TA, Shakya R, Pitarresi JR, Swanson B, McQuinn CW, Loftus S, et al. IL-6 and PD-L1 antibody blockade combination therapy reduces tumour progression in murine models of pancreatic cancer. Gut. 2018;67(2):320-32.
29. Downward J. RNA interference. BMJ. 2004;328(7450):1245-8.
30. Damm-Welk C, Fuchs U, Wossmann W, Borkhardt A. Targeting oncogenic fusion genes in leukemias and lymphomas by RNA interference. Semin Cancer Biol. 2003;13(4):283-92.
31. Ge Q, McManus MT, Nguyen T, Shen CH, Sharp PA, Eisen HN, et al. RNA interference of influenza virus production by directly targeting mRNA for degradation and indirectly inhibiting all viral RNA

transcription. Proc Natl Acad Sci U S A. 2003;100(5):2718-23.
32. Gitlin L, Karelsky S, Andino R. Short interfering RNA confers intracellular antiviral immunity in human cells. Nature. 2002;418(6896):430-4.
33. Coburn GA, Cullen BR. Potent and specific inhibition of human immunodeficiency virus type 1 replication by RNA interference. J Virol. 2002;76(18):9225-31.